Engineering Solid Mechanics 11 (2023) 325-338

Contents lists available at GrowingScience

Engineering Solid Mechanics

homepage: www.GrowingScience.com/esm

Fracture toughness evaluation of zeolite/polyurethane-filled woven panels

Hamid Safari[a*], Mehdi Karevan[b] and Hassan Nahvi[b]

[a]*Department of Mechanical and Aerospace Engineering, Ira A. Fulton Schools of Engineering, Arizona State University, Tempe 85287, Arizona, United States*
[b]*Department of Mechanical Engineering, Isfahan University of Technology, Isfahan 8415683111, Iran*

ARTICLE INFO

Article history:
Received 20 September 2022
Accepted 12 January 2023
Available online
12 January 2023

Keywords:
Fracture toughness
3D woven fiberglass fabric
Composite sandwich panels
Single Edge Notched Bend
Energy of fracture
Crack

ABSTRACT

Recently, due to their extraordinary strength-to-weight ratio and multi-functional applications, three-dimensional woven fiberglass sandwich structures have become a well-received topic by researchers and manufacturers. Nevertheless, using light and foam absorber materials as injected fillers within sandwich cores can improve their overall mechanical performance and, in particular, their fracture toughness behavior. This study evaluates the fracture toughness of three-dimensional woven fiberglass sandwich panels filled with natural nano-structured zeolite/polyurethane foams injected between their parallel panels. The Single-Edge Notched Bend test was carried out to understand the effect of the injected foam on the mode-I fracture toughness response. It is demonstrated that the polyurethane foam reinforced with natural nano-structured zeolite particles highly improved the fracture toughness of sandwich core panels. It was found that the presence of vertical glass yarns within the sandwich panel gallery resulted in a significantly higher toughness compared with typical sandwich panels of no reinforcing vertical columns confirmed by the crack propagation and observed failure mode. The SEM and EDX analyses were used to better understand the correlations amongst the specimen morphology, the cracks behavior, and the toughness exhibited by the fabricated specimens.

1. Introduction

The increasing use of more advanced composites has been shown in many structural applications due to their favorable and tunable properties. For instance, high weight-to-strength ratio materials are needed to reduce weight and increase the long-term performance of structures under static or dynamic loading. Three-dimensional (3D) woven fiberglass sandwich panels are rather a new class of composites that can be used as structures in many industries, such as interior bodies in passenger cars. Moreover, their intrinsic mechanical properties, ease of fabrication, and scale-up manufacturing make them attractive candidates to be utilized in various industries. It is easily understood from their targeted applications many structures are often subjected to various loading events. The latter suggests that the characterization of the fracture and crack mechanics in 3D woven composite sandwich panels have proven to be critical to provide a safer design and a better stress analysis of the panels due to the possibility of fracture caused by applied loads. Whilst composites, including the 3D woven-based ones normally exhibit their engineered and, thus, improved performance, it has been recently considered to reduce the cost of reinforced composites by incorporating a proportion of cheaper materials such as polyurethane to attain a greater reinforcing efficacy against the final costs and weight. Accordingly, the fracture toughness parameters are expected to play a crucial role in the overall mechanical response of composites and, thus, need to be better understood, and, in particular, in the case of less-known modified composites. As frequently reported elsewhere, the mechanical performance of such composites mainly depends upon fiber content, fiber orientation, fiber-to-matrix bonding, and a suitable arrangement of the fibers (Sreekala et al., 2002). These configurations can enhance composites through-thickness strength, impact resistance, and tear resistance. The high risk of delamination cracking in composites either compromises the exploitation level of their use in engineering applications or limits their application envelope to structural components. The delamination behavior and crack growth

* Corresponding author. Tel.: +16026327886
E-mail addresses: hsafari@asu.edu (H. Safari)

ISSN 2291-8752 (Online) - ISSN 2291-8744 (Print)

doi: 10.5267/j.esm.2023.1.005

resistance of composites, therefore, should be studied for a deeper understanding of the mechanisms involved in delamination cracking.

Many studies have been reported addressing the fracture properties and damage resistance of woven composites employing experimental tests as well as numerical and analytical models in recent years. Byun et al. (1990) conducted a finite element analysis on mode-I delamination of a three-dimensional fabric composite to determine the influence of through-the-thickness fibers on crack driving force as a function of crack length. Their parametric study revealed that increasing the z-axis fiber stiffness reduced the strain energy release rate. Guénon et al. (1989) experimentally determined the interlaminar fracture toughness of 3D orthogonal interlocked fabric composites by using a double cantilever beam specimen. The results exhibited that the through-thickness fibers created a ten-fold increase in the interlaminar toughness and an improvement in the in-plane fracture toughness performance of the specimens. Mouritz et al. (1999) assessed the mode-I fracture toughness properties of advanced textile fiberglass composites and the effects of complex fiber distribution on mechanical properties. They showed that toughening in a specific type of textile composite was caused by extensive crack branching in the interlaminar crack. Tong et al. (2002) studied the effect of fiber addition on the through-thickness of composites to increase the laminate toughness. It has been further shown that the lack of through-thickness reinforcements in layered composites causes weaknesses in their fracture properties. Another report (Shivakumar Gouda et al., 2013) revealed the investigation of the fracture behavior of a high-silica fiberglass-reinforced composite under the full range of in-plane loading conditions, both experimentally and numerically. For instance, Gouda et al. (2011) addressed the mode-I fracture behavior of glass-carbon fiber-reinforced polymer composites based on experimental and finite element analysis. They showed the cracked specimens were tougher along the fiber orientations than across the fiber orientations. Callus et al. (1999) performed tensile experiments at low loadings to investigate the crack initiation in the elastic mode. Their study illustrated that cracks were typically formed at low strains within the resin-rich channels between the fiber tows and around the through-thickness binder yarns in the composites. The results further indicated that this cracking damage did not alter the tensile properties. The study, moreover showed that the elastic modulus was reduced at higher applied tensile stresses due to the inelastic tow straightening and cracking around the most heavily crimped in-plane tows. Other researchers also have presented analytical and experimental research on the crack formation of vertical-yarn reinforcement in 3D orthogonal woven CFRP composite panels. They showed the overall response of the structure and investigated the failure mechanisms of 3D orthogonal woven CFRP composites on the macro- and microscale (Tan et al., 2000a; Tan et al., 2000b). Danielsson (1996) analyzed the energy absorbent and mechanical failure mechanisms of a rigid foam core material for sandwich construction and demonstrated that cell size and size distribution influenced the energy absorbent capability and the stress intensity factor. It was demonstrated that the cell size and size distribution, combined with density, strongly contributed to the properties mentioned earlier. Stewart et al. (2010) studied the mechanical and fracture properties of sandwich composites using nanoparticle reinforcements and determined the fracture toughness of specimens using the Single-Edge Notched Bend (SENB) test. Their work well represented the fact that the foam filled with pristine nanoparticles resulted in substantial enhancement in the mechanical properties. Nevertheless, the study confirmed the presence of the reinforcing phase lowered the fracture toughness of the specimens. Rao et al. (2009) focused on investigating the effect of vertical yarns on the stiffness, failure, and strength of 3D woven composites utilizing the Tsai–Hill criterion. Their models were then modified to study the effect of including Z-yarns on changes in stiffness and strength properties. De Souza et al. (2012) investigated the effect of the sample pre-cracking method and notch geometry on the plane-strain fracture toughness. They quantitatively studied the obtained plane-strain fracture toughness (K_{IC}) values, followed by a qualitative examination of its effect on the Moiré fringes observed using photoelasticity. They exhibited a 95% significance level, and the K_{IC} values were affected by the pre-cracking method, which employed the most conservative values obtained when natural pre-cracks were introduced by tapping on a razor blade. Alsaadi et al. (2018) fabricated polymer composites loaded with 5 to 20 wt% of toughening fillers to evaluate the varying crack inclination angles and, thus, the mode-I loading conditions. The study recorded the maximum values of fracture toughness mode-I at the particle content of 5 wt%. Therefore, it could be easily understood from the literature that the addition of fillers can be considered as a governing factor in improving fracture behavior. Fishpool et al. (2013) evaluated the optimum architecture for improving delamination resistance in 3D woven carbon fiber-reinforced epoxy composites in mode-I using the double cantilever beam test method. An orthogonal weave was most effective at resisting delamination propagation in mode-I comparable to the layer-to-layer architecture. In another report, Tan et al. (2012a, 2012b) determined the mode-I interlaminar fracture toughness of Vectran-stitched laminated composites based on the combination of computational and experimental approaches. They showed interlaminar fracture toughness increased as the stitch thread thickness and density increased. Tarfaoui and Hamitouche (2012) focused on the mode-I interlaminar fracture toughness for glass/vinylester-based composites. They mentioned that a finite element model would be successful in reproducing qualitatively the crack initiation and propagation in the unreinforced and 3D reinforced samples. Srivastava et al. (2017) improved the fracture toughness of CFRP composites by the incorporation of nanofillers. Alsaadi and Erklig (2017) analyzed the effect of silica nanoparticle-filled polymer composites on the mixed-mode fracture toughness of the SENB samples with crack angles of 30°, 45°, 75°, and 90° to calculate the fracture parameters. They elucidated that the addition of nano-silica affected the composite fracture toughness. Ji et al. (2014) examined carbon fiber-reinforced polymer matrix composites and showed the performance of interlaminar fracture toughness of composites. Their study described that the delamination for all specimens extended slowly and stably, and the presence of the fibers in the composite matrix depended on their directions, fiber weight percent, and the fiber-matrix interaction. They further showed the physical and chemical properties of fiber dictated the overall composite properties. Zhang et al. (2015) developed alumina-reinforced 3D alumina fiber mats to elucidate the contribution of multi-walled carbon nanotubes and alumina fibers in

enhancing the fracture toughness of the composite. Göktaş et al. (2017) examined the improved interlaminar fracture toughness of multilayered 3D glass/epoxy textile composites when various stitching techniques introduced through-thickness reinforcements. Other studies performed on the mode-I fracture toughness of 3D stitched composites have been conducted elsewhere (Mouritz et al., 1999; Tong et al., 2002; Mouritz et al., 2000; Dransfield et al., 1994; Sharma & Sankar, 1997; Solaimurugan & Velmurugan, 2008). It can be clearly understood from the literature that only a few studies have been performed on the fabrication of 3D woven fiberglass-reinforced composite panels, and no research has been conducted with a focus on characterizing the fracture toughness behavior of this class of composites. Moreover, since reinforced polyurethane foams are expected to become even more brittle compared to neat foams, there is a need to represent the synergistic effects of such foams when used within 3D woven fiber composite panels; this can further provide extended applications of reinforced polyurethane foams when combined with other structural composites.

In a general approach to fracture toughness tests, there are three different modes of fracture loading configurations. The mode-I requires that the applied load be in the normal direction to the crack plane. In mode-II, the load is applied along the length of the crack plane. Finally, in the case of mode-III, the load is applied across the width of the crack plane. The SENB (three-point bending) and compact tension are two different configurations for the test sample. The three-point bending specimen has the initial crack located at the midsection on the opposite side from the point where the midsection load is applied, with opposing points of force located at each end on the same side as the crack. A compact tension specimen is oriented using applied loads on each side of the crack in a way that extends the width of the crack. The SENB test has been used to characterize the stress intensity factor or fracture toughness of composites and determine the fracture performance of composites. This method requires a pre-crack by cutting a crack in the edge of a specimen. Standard test methods for fracture mechanics testing of plastics and polymers are available.

In this research, a novel approach to address the sandwich panel delamination issues aiming at increasing the fracture toughness by the adoption of through-thickness reinforcing techniques such as 3D woven sandwich panels is hypothesized and experimentally examined. Crack propagation can also be another issue considered in experimental studies. The energy of fracture by damage while the crack extends as a fracture measure was reviewed. The results of these studies probably make the best decision to use 3D composites in specific applications.

This study evaluated the fracture toughness behavior of a new type of 3D woven fiber sandwich composite filled with reinforced polyurethane using SENB specimens. Tests were carried out on three-point bend loading to gain a better insight into the effect of weaving architecture and filler addition to the sandwich panel on the damage mechanisms, crack propagation resistance, and fracture toughness of a 3D woven composite. The fracture toughness results of plain and natural nano-structured zeolite/polyurethane-filled 3D woven fiberglass composite sandwich panels are compared. The results show that plain 3D woven sandwich composites have lower damage resistance than those filled with natural nano-structured zeolite/polyurethane. The results of the present study illustrate a methodology in the fabrication and characterization of 3D woven panels filled with reinforced foams exhibiting enhanced fracture toughness to be used in statically or dynamically loaded structures as seen in automotive bumpers, marine and space vehicle bodies and parts, and construction industries.

2. Materials and Methods

In this study, the 3D woven E-fiberglass fabric (200 gr), and the epoxy resin (grade LR-2025) were cured with hardener (HE 1515) for a resin-hardener ratio of 10:1 by weight to fabricate the SENB specimens. Moreover, polyurethane foam (supplied by a local retailer) consisting of polyol and isocyanate with a one-to-one mix ratio and natural nano-structured zeolites were mixed for the fabrication of the natural nano-structured zeolite/polyurethane-filled 3D woven fiberglass specimens. To prepare the nano-structured zeolite/polyurethane core specimens, 5-20 wt% of zeolite filler was added to the polyol-isocyanate mixture and mixed using a mechanical mixer at 1300 rpm for 17 min. The compound was manually injected into the sandwich panel core to fabricate the final filled sandwich panels. Fig. 1 indicates a plain composite sandwich panel specimen made of epoxy resin and 3D woven fiberglass fabric.

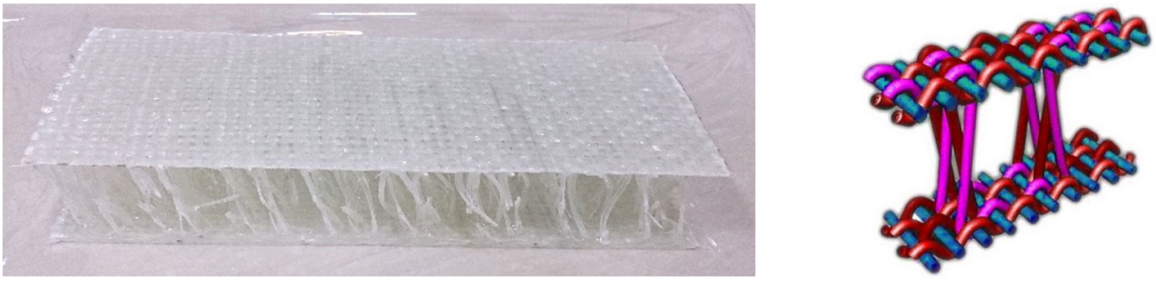

(a) (b)

Fig. 1. Plain composite sandwich panel specimen made of epoxy resin/3D woven fiberglass fabric (a) fabricated 3D woven sandwich panel sample and (b) a schematic of 3D woven fabric.

2.1. Morphological Properties

2.2.1. SEM and EDX of nano-structured zeolite/polyurethane-filled composites

Scanning Electron Microscope (SEM) was utilized to study the phase morphology of nano-structured zeolite/polyurethane-filled specimens on a Philips XL30 equipment (Netherlands). The specimens were fractured using liquid nitrogen to avoid plastic and possible secondary mechanisms altering the surface morphology. The cross-sectional area of the fractured surface of the specimens was examined following the gold sputtering of the fractured surface for 90 s. Additionally, the chemical characteristics were investigated employing Energy Dispersive X-Ray (EDX) analysis. The SEM images indicated a porous nature, a rough surface, and morphology distributions with nonhomogeneous and irregular shapes directly dependent upon the milling process, as shown in Fig. 2. The SEM images also represented the presence of smaller particles with spherical shapes with a dimension of 100 to 1000 nm. The SEM images in Fig. 2 reveal the dispersion quality of zeolite against the filler weight fraction in the polyurethane foam.

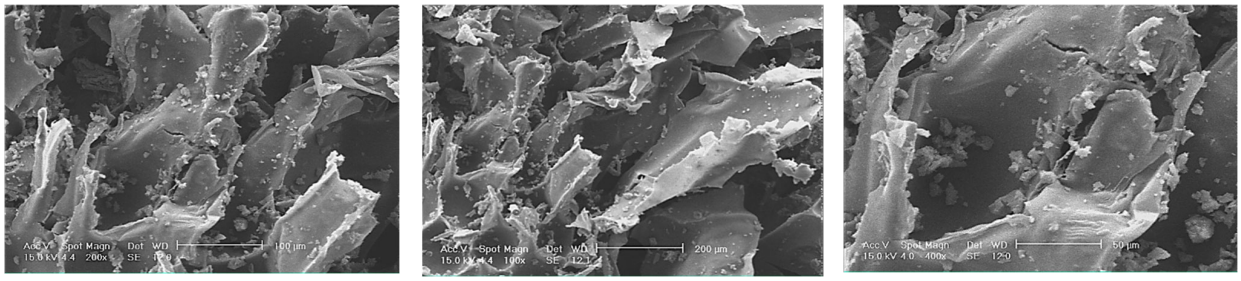

(a) (b) (c)

Fig. 2. Dispersion of zeolites at the loading of (a) 5 %, (b) 10 % and (c) 20 wt% in the polyurethane matrix.

The zeolite from aluminosilicate minerals was found by indicating the high concentrations of key elements such as Al, Si, and O and the presence of other elements such as Na, Mg, K, and Ca. The highly crystalline structure and thermal stability of natural zeolites, together with unique ion exchange, adsorption properties, a large surface area, and porosity, make them suitable for a wide range of applications as an additive or catalyst (Nizami et al., 2016). Fig. 3 shows the EDX spectroscopy of the studied natural nano-structured zeolite. Table 1 gives the weight fraction and atomic% of elemental composition in the natural nano-structured zeolite used in this work.

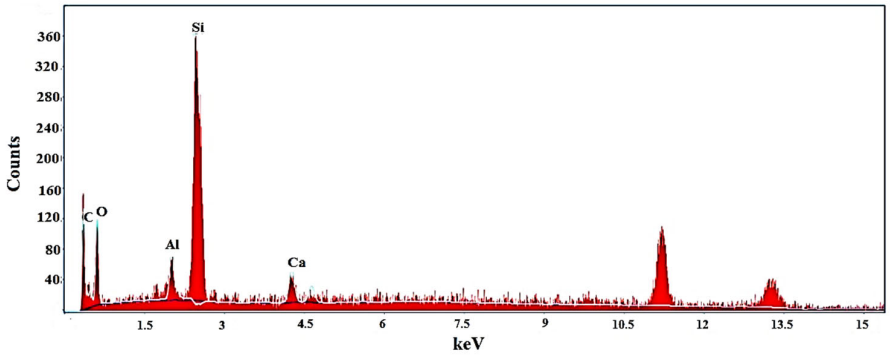

Fig. 3. EDX spectrum of natural nano-structured zeolite.

Table 1. Characterized chemical elements of natural nano-structured zeolite by EDX analysis.

Element	Weight %	Atomic %
C	0.72	1.25
O	50.47	49.42
Al	32.10	41.57
Si	7.22	4.02
Ca	9.45	3.61

2.2. Three-point SENB mode-I fracture characterization

The three-point SENB mode-I fracture tests of specimens were performed using a universal testing machine (SANTAM co., Iran) with a load cell of 50 kN. Each test was performed at a cross-head speed of 2 mm/min. The test was repeated using four specimens in the case of each reinforced system. The average load-deflection curves for four specimens of each type of composite were plotted, and the force for the calculation of fracture toughness was recorded by calibrating a testing system

following the ASTM D5045-99 standard (ASTM, 2007). The test fixture was set up so that the line of action of the applied load passed midway between the support roll centers. For each specimen, the test was carried out until the crack grew through the entire specimen.

The center-cracked panels were used to evaluate the fracture toughness of the composites. Before testing, a pre-crack was created at the mid-span on the tension side of the specimens using a razor blade. The sharp-crack condition at the tip of the crack in a specimen of adequate size to give linear elastic behavior and the validity of the determination of the fracture toughness (K_{IC}) value was introduced per the ASTM D5045-99 standard (ASTM, 2007). Tests were carried out at room temperature 21±2 ºC. A schematic representation of loading the SENB specimen and adopting geometry is given in Fig. 4.

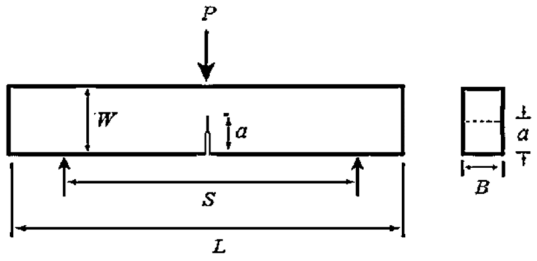

Fig. 4. A schematic representation for loading the SENB specimen (ASTM, 2007)

In this study, rectangular samples were prepared with dimensions of 150×24×50 mm^3 (L×B×W). A pre-crack with the length a = 24 mm was cut, whereas the span length S = 110 mm was selected by the test fixture supports. The plane-strain fracture toughness, K_{IC}, was calculated according to standard ASTM D5045-99 for SENB according to Eq. (1):

$$K_{IC} = \frac{P_Q \times S}{BW^{3/2}} f(a/W) \tag{1}$$

where P_Q is the calculation force, and B and W are specimen dimensions. The function $f(a/W)$ is given by Eq. (2) (ASTM, 2007):

$$f(a/W) = 3\sqrt{a/W}\,\frac{1.99-(a/W)(1-a/W)[2.15-3.93(a/W)+2.7(a/W)^2]}{2(1+2a/W)(1-a/W)^{3/2}} \tag{2}$$

The property K_{IC} characterizes the resistance of a material to fracture in the presence of a sharp crack under specified loading, such that the plane strain state is approached for stress near the crack front (Zimmermann et al., 2010). The crack-tip plastic region is small compared with the crack size and specimen dimensions in the constraint direction (Anderson, 2005). A K_{IC} value indicates a lower limiting value of fracture toughness and can be used to estimate the relation between failure stress and defect size (ASTM, 1991). The energy of fracture, γ_{wof}, was calculated by the work done by the testing instrument on a SENB specimen until a single crack propagates completely. The energy of fracture corresponds to the area under the curve of load, P, versus load point displacement, d, divided by the total projected surface area, A, of the two fracture surfaces formed by Eq. (3) (Williams et al., 2003),

$$\gamma_{\text{wof}} = \left(\int \text{P. d (d)}\right) / 2\text{A} \tag{3}$$

At the onset of crack propagation, the stored elastic strain energy not only depends on the material's toughness, K_{IC}, and its Young's modulus, E, but also on geometric factors such as the specimen dimensions and notch depth, and the stiffness of the testing equipment, including the bending supports (Nakayama et al., 1981). During the fracture process, this potential energy was transformed into surface energy and sometimes dissipated by the interaction of the crack with the microstructure (Peret & Rodrigues, 2008). Mode-I strain energy release rate (G_{IC}) of composite sandwich panels was calculated using the SENB test by applying Eq. (4):

$$G_{IC} = \frac{(1-\upsilon^2)K_{IC}^2}{E} \tag{4}$$

where, υ is Poisson's ratio, which for fiberglass/resin epoxy composite varies from 0.30 to 0.25 depending upon different fiber volume fractions of 30% to 70% (Sudheer et al., 2015), K_{IC} is the fracture toughness, and E is the bending elastic

modulus, which was calculated according to the three-point bending test on the broken samples from the SENB test using Eq. (5) (ASTM, 2007),

$$E = \frac{S^3 m}{4BW^3} \tag{5}$$

where m is the slope of the force-deflection graph, B is the thickness of the specimen with width W, and S is the support span. The thickness of the specimen was 24 ± 0.8 mm, whereas its width was 50 ± 1.5 mm, thereby maintaining the W/B ratio greater than two as a requirement for the plane strain condition.

3. Results and Discussion

3.1. Three-point bending tests of SENB

The load corresponding to a 2.5% apparent increment of the crack extension was established by a specified deviation from the linear portion of the diagram. The K_{IC} value was obtained from this load by using equations that have been derived based on Linear Elastic Fracture Mechanics (LEFM) on specimens (ASTM, 2007). All tests were validated using geometrical constraints to induce plane-strain during crack propagation. Therefore, all results were reliable and valid for the determination of K_{IC}. An average statistical value was applied to compare the K_{IC} values. Considering the 95% significance level, the K_{IC} values were affected by pre-cracking. Since the test was performed only with single-notched specimens, it was noticed that the relatively rough notching procedures produced several microcracks in the polymer matrix close to the notch root, which operated as natural pre-cracks (De Souza et al., 2012). A similar elaboration can be provided to verify the application of the SENB method for measuring the fracture toughness of 3D woven composites; however, it has been shown that the K_{IC} value varies with changes in the notch width (Pabst, 1974). Fig. 5 depicts the experimental setup of plain 3D woven composites under the three-point SENB test.

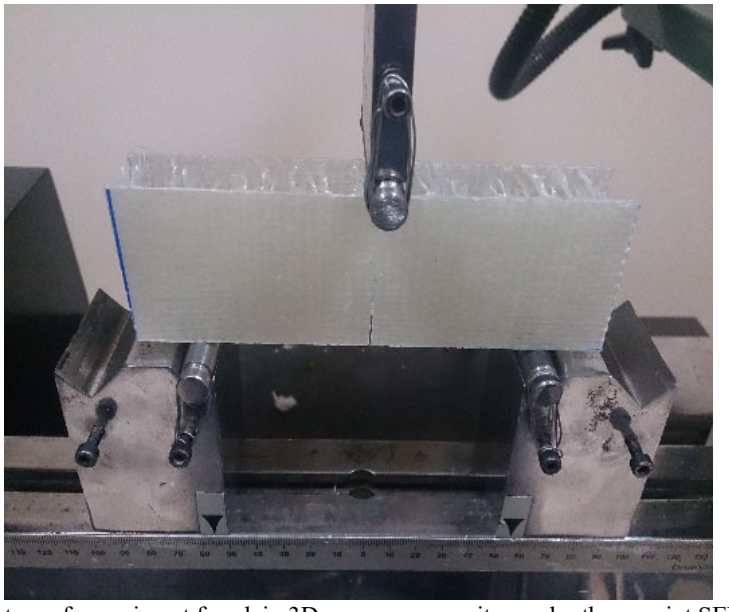

Fig. 5. Set up of experiment for plain 3D woven composites under three-point SENB test.

The sandwich composites demonstrated in Figs. 6 and 7 represent linear elastic behavior up to the initiation of cracking open at the tip of the crack. Beyond this point, the specimens showed a slight reduction in load. All specimens represented the evidence of damage or a sudden load drop before failure. Regardless of the composition system, the material failed in a ductile mode. The effect of injecting polyurethane/zeolite was correlated with the increase in the maximum load obtained in these specimens. The average load-displacement curves for four SENB specimens of each type of the various composites are displayed in Figs. 6 and 7.

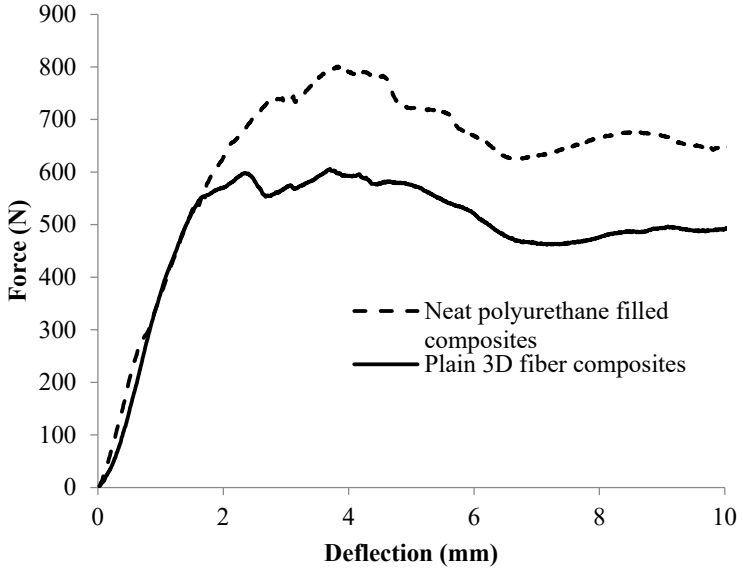

Fig. 6. Average load-displacement curve of plain 3D fiber composites and neat polyurethane-filled composites for SENB specimens.

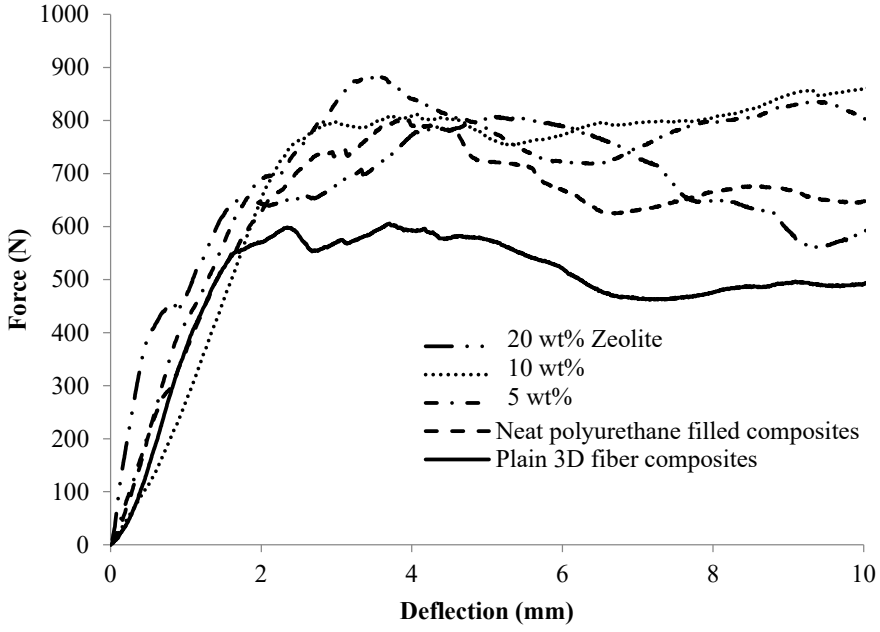

Fig. 7. Three-point SENB force-displacement curves of plain 3D fiber as well as zeolite/polyurethane-filled composite sandwich panels as a function of zeolite wt%.

The values of average fracture toughness K_{IC} of the four specimens of each composite type, together with the corresponding load P_Q and energy of fracture γ_{wof} of the types of 3D woven composites under three-point SENB loading as a function of wt% zeolite, are summarized in Table 2.

Table 2. Fracture properties of the types of 3D woven composites for three-point SENB test as a function of wt% zeolite.

Three-point SENB specimens	P_Q (N)	K_{IC} (MPa. $m^{1/2}$)	γ_{wof} (kJ/m^2)
Plain 3D fiber composites	598.5 ± 16.8	19.84 ± 0.5	5.85
Neat polyurethane-filled composites	797.8 ± 9.7	24.45 ± 0.8	15.07
Zeolite wt%			
5	881.6 ± 70.5	29.20 ± 0.4	19.35
10	799.5 ± 55.9	26.48 ± 0.6	19.46
20	694.5 ± 62.5	23.01 ± 0.3	14.07

It is also clear from Table 2 that the highest and lowest peak loads were found in the cases of 5 wt% zeolite/polyurethane-filled composite and plain composite, respectively. The plane-strain fracture toughness of the investigated plain 3D woven composites was measured to be around 19.84 MPa.m$^{1/2}$. As seen in Table 2, this value in the case of neat polyurethane-filled composites was determined to be around 24.45 MPa.m$^{1/2}$. Moreover, in the case of 5 wt%, 10 wt%, and 20 wt% zeolite/polyurethane composite systems, the fracture toughness values were obtained at 29.20, 26.48, and 23.01 MPa.m$^{1/2}$, respectively. The results verified the improved fracture toughness of zeolite/polyurethane-filled composites compared to that observed in the case of plain composites, shown by the 50% increase in the fracture toughness value. One probable reason is that the zeolite/polyurethane network has a pining effect on crack growth, inhibiting its propagation. Furthermore, it is suggested that the accurate and prescribed ratio of the polymer components (i.e., in two or three-part resins) could be interfered by the surface of the fillers due mainly to the filler/polymer interfacial interactions (Karevan, 2022). Fig. 8 illustrates the variations achieved in G_{IC} after adding 5-20 wt% of natural nano-structured zeolite/polyurethane in plain sandwich panels. Lower and upper limits of G_{IC} in Fig. 8 were calculated using $\upsilon = 0.25$ and 0.30 in Eq. (4). The mean G_{IC} increased nearly 2-fold relative to that of the plain sandwich panel after adding neat polyurethane and 5-20 wt% of natural nano-structured zeolite/polyurethane. The findings could be attributed to the combined effect of thickness throughout the fiber-zeolite-foam core-filled composite stereology and the unique debonding/pull-out mechanisms observed in SEM images. Table 3 indicates strain energy release rates for some types of composites under three-point SENB test.

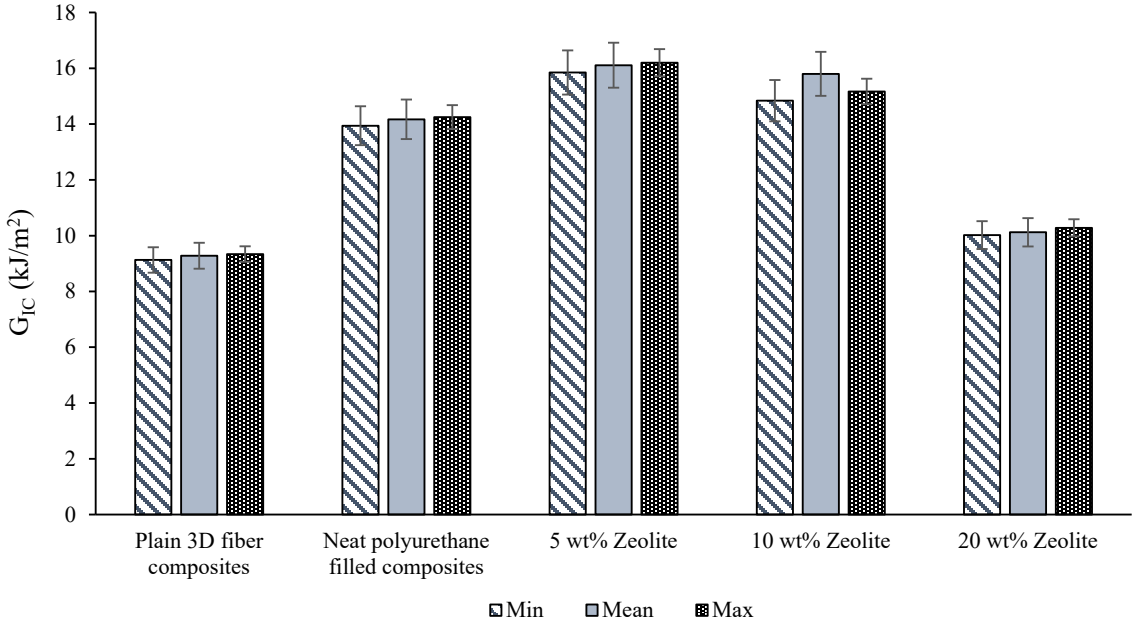

Fig. 8. Mode-I strain energy release rate mean values of plain 3D fiber as well as zeolite/polyurethane-filled composite sandwich panels as a function of zeolite wt% (Min and Max bars in accordance with $\upsilon = 0.25$ and 0.30, respectively) .

Table 3. Strain energy release rates for some types of composites under three-point SENB test.

Three point SENB specimens	Strain energy release rate G_{IC} (kJ/m^2)
CFRP + 4 wt% SiC nanosilica (Carolan et al., 2016)	1.170±0.13
CFRP + 8 wt% CSR (Carolan et al., 2016)	1.680±0.12
CFRP + 8 wt% CSR+ 4 wt% SiC nanosilica (Carolan et al., 2016)	1.851±0.13
CFRP (Cholake et al., 2016)	0.89±0.15
CFRP+ 5 wt% short milled carbon fibre (Cholake et al., 2016)	0.98±0.12
CFRP+ 5 wt% short milled carbon fibre (Cholake et al., 2016)	1.16±0.15
Sandwich panel (foam+0.1 wt% SiC) (Stewart et al., 2010)	0.561±0.10
Sandwich panel (foam+0.3 wt% SiC) (Stewart et al., 2010)	0.337±0.10
Sandwich panel (neat foam) (Stewart et al., 2010)	0.142±0.15
(present study as follows)	
Plain (3D woven fiber) composites	8.51±0.05
Neat polyurethane filled composites	15.16±0.04
Polyurethane filled composites + 5 wt% Zeolite	14.62±0.06
Polyurethane filled composites + 10 wt% Zeolite	14.5±0.06
Polyurethane filled composites + 20 wt% Zeolite	9.29±0.05

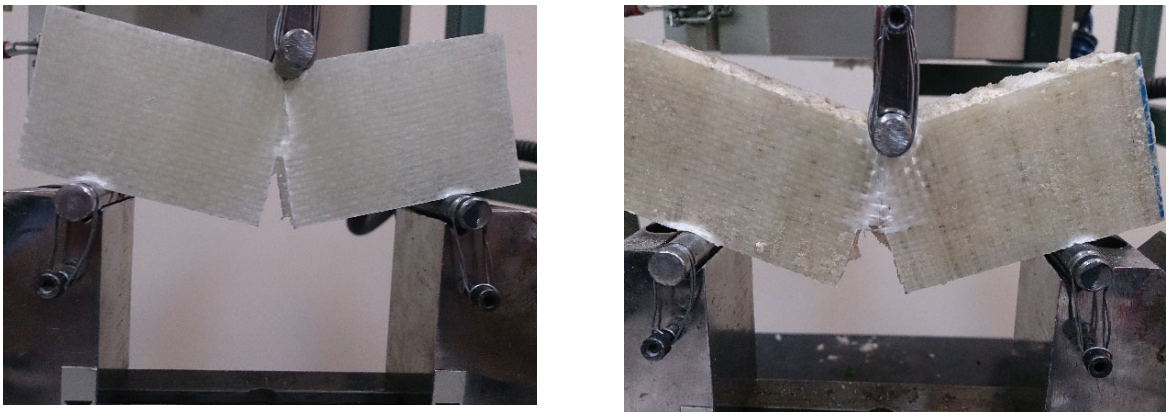

(a) (b)

Fig. 9. Crack propagation under three-point SENB test in the case of (a) plain 3D fiber composites, and (b) zeolite/polyurethane-filled composites.

The results show that the resistance of the fabricated composites to the propagation of cracks through a 3D woven fiber composite is enhanced by using vertical or through-thickness yarns as bridging or connecting factors to the composite skin layers. The failure mechanisms of common configurations of skins, such as debonding at the fiber-matrix interface, fiber fracture, and fiber pull-out under tensile loading in three-point bending, are observed in Figs. 9(a) and (b). As seen in Fig. 9, the entire straight-through pre-crack function as a nucleus for unstable propagation is exhibited. The through-thickness fibers resist the applied crack-opening forces and, consequently, reduce the interlaminar stresses at the crack tip. The delamination of a composite under mode-I conditions resulted in the gradual pull-out of the fibers with increasing opening displacement. The pull-out as a two-phase occurrence was initiated by stretching the fiber elastically and debonding gradually from the laminate. After complete debonding, fiber pull-out is thought to be controlled through the friction of the fibers with the matrix. The first matrix cracking occurred, and fibers fracture followed at the maximum loading level P_{max}. All load-deflection curves exhibited an initial linear response that became progressively non-linear as the load dropped, which indicated fast, and stable crack growth because additional crack opening displacement was not required for the crack propagation. It is suggested that the crack initially propagated in a stable and eventually unstable manner at maximum load. As the strain increased with continued loading, cracks formed, and the amount of damage increased until a complete fracture. It is believed that several microcracks joined together to form a major crack, ultimately leading to a fracture by separation. The damage was, however, considerably larger in the case of the pre-crack introduced by the cutting blade. These observations were in good agreement with other failure analysis investigations as reported elsewhere (Greenhalgh, 2009). For a better understanding of the nature of this damage, further structural observation is proposed using SEM fractography analysis.

3.2. Fractography

The main advantage of conducting a fractography analysis using SEM is the excellent resolution obtained, allowing detailed evaluations of the fracture process. The fracture surface of the SENB specimens was examined using SEM experiments to elucidate the toughening mechanism of zeolite/polyurethane-filled and plain sandwich panels at different magnifications after the fracture surfaces of the specimens were gold-sputtered. The fracture surface of SENB specimens usually has three different regions: the pre-crack zone, the process zone, and the fast fracture region (Yee & Pearson, 1986). The edge of a razor blade produces the pre-crack. During the test, cracks first undergo stable sub-critical growth in the process zone and propagate instability in the fast-fracture region. The process zones are usually evaluated to understand failure mechanisms because the material resistance to cracking in these regions reflects fracture toughness properties. In the zeolite/polyurethane-filled foam core, due to their porous structures, zeolite particles were taking part in absorbing more energy for crack initiation. This supported the increment observed in the G_{IC} after the addition of 5 wt% zeolites. However, in the case of specimens loaded with 10-20 wt% of particles, the zeolite agglomeration could corroborate the brittle structure and, thus, the observed decrease in the fracture toughness of the specimens. The fracture surfaces shown in Fig. 10 represent the mechanical entanglement of fibers and fillers acting as obstacles to crack propagation and delamination in this region. Indeed, the entangled fibers and fillers contribute to the interlocking (intralaminar) feature that enhances the fracture toughness of the composite. Such regions act as crack stoppers before fibers undergo debonding and pull-out, leading to ductile fracture. The fracture surfaces of zeolite/polyurethane-filled 3D woven fibers are shown in Fig. 10.

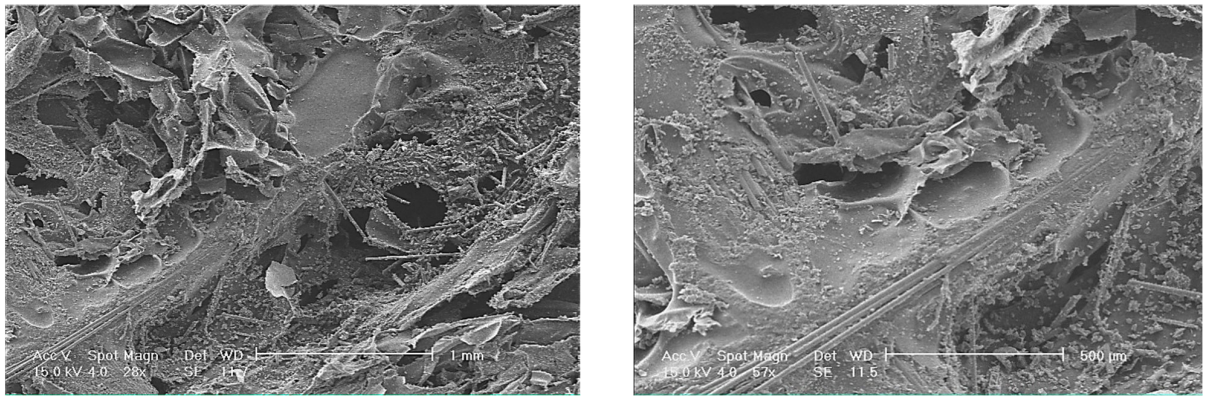

(a) (b)

Fig. 10. SEM images of fractured surface of thickness throughout fibers-zeolite-polyurethane-filled core.

The SEM micrographs of fractured surfaces in the case of resin fibers are shown in Figs. 11(a) and (b). The evidence of matrix cleavage, matrix cracking, fiber debonding, fiber fracture, the pull-out of fibers, and the separation of the matrix and fibers is clearly shown. The images support the presence of good bonding at the interface of the fiber/matrix. Cracks were formed by the coalescence and growth of fiber detachment and micro-cracks in the matrix. Multiple fractures of fiber, instantaneous fractures of fibers, and all transverse fibers well bonded with the matrix are additional features shown by the SEM micrographs. Moreover, the mechanism of the crack propagation process along the fiber/matrix boundaries with visible degradation of the interface is illustrated in Fig. 11. Multiple areas of crack initiation are visible, resulting from the loss of adhesion that, in turn, leads to the damage of the composite when combined.

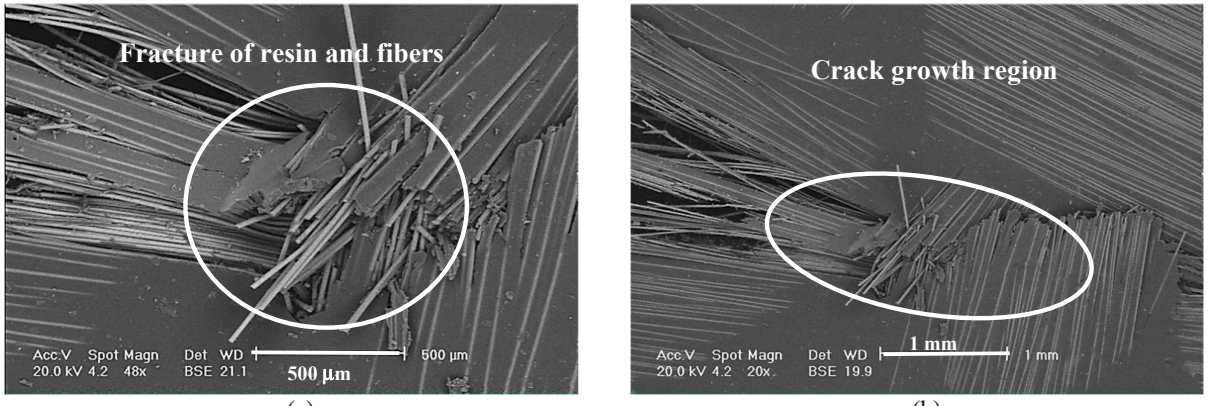

(a) (b)

Fig. 11. SEM images of fracture and crack propagation region of fibers and resin epoxy matrix.

The fractured and damaged regions of the composites in the crack tip zone are visible as shown in Fig.11. It could be understood that microcracks are formed. The increase in load causes the initiation of the rupture in the composite. Fig. 12 also exhibits the fracture surfaces between the fiber and resin matrix in the crack tip zone.

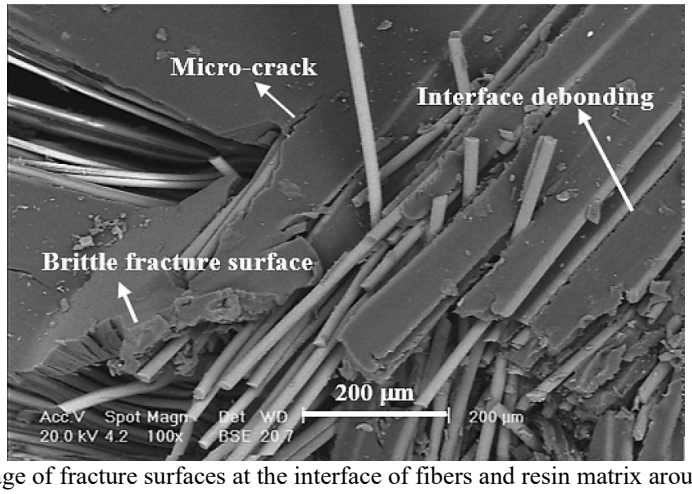

Fig. 12. SEM image of fracture surfaces at the interface of fibers and resin matrix around crack tip zone.

3.3. Fourier-transform infrared (FT-IR) spectroscopy

The FT-IR spectroscopy of the composites was addressed for the structural and chemical analyses. The FT-IR spectrums were plotted as shown in Fig. 13. The spectrums for all zeolite/polyurethane composite specimens showed very similar intensities and positions of the absorption bands, indicating that the overall structure of all specimens contains the same functional groups. However, the variations can be attributed to different Al-O, Si-O, and Si-O-Al bonds.

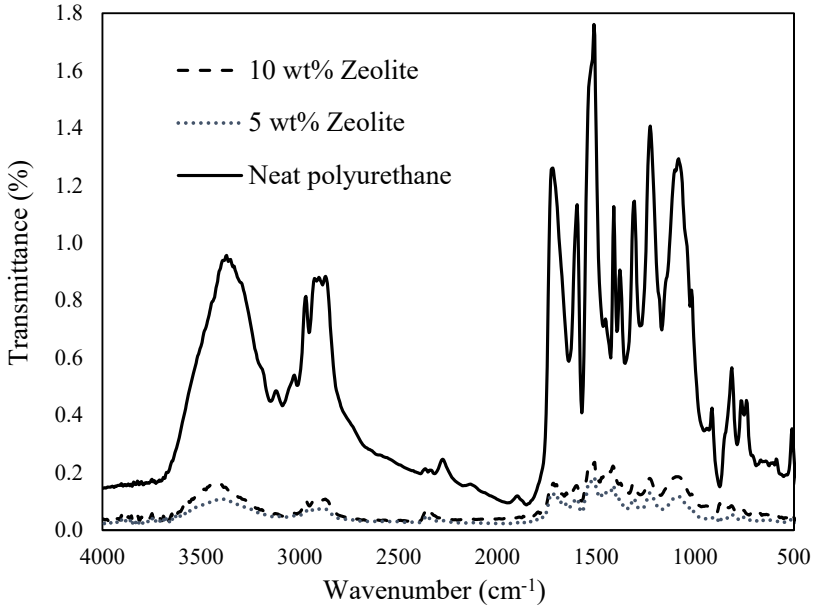

Fig. 13. FT-IR spectrums zeolite/polyurethane-filled composite as a function of zeolite wt%.

4. Conclusions

A new composite material was created by incorporating natural nano-structured zeolite/polyurethane into 3D woven fiberglass composite sandwich panels. The SENB specimens were designed, fabricated, and tested in mode-I fracture to evaluate mechanical performance. The fracture toughness efficiency was investigated by injecting reinforced polyurethane into the galleries of the plain 3D woven composites. The structure reactions were provided for energy absorption to create the new surfaces by crack opening, contributing to a 230% increase in the energy of fracture. The experimental results further indicated that the K_{IC} values increased by 50% when composite panels were filled with zeolite/polyurethane at a zeolite content of 5 wt%. Moreover, the findings showed that the strain energy release rate increased by 110% when the polyurethane foam was used in the sandwich core. The fractured surfaces and crack opening observations of the 3D woven composite specimens were addressed to gain insight into failure under three-point loading conditions. The results supported the view that the mode-I fracture surface was indicative of ductile failure with a relatively smooth and flat matrix fracture corroborating debonding between fibers and matrix with the fracture of fibers.

Declaration of Conflicting Interests

The authors declared no potential conflicts of interest with respect to the research, authorship, and/or publication of this article.

References

Alsaadi, M., Erkliğ, A., & Bulut, M. (2018). Mixed-mode I/III fracture toughness of polymer matrix composites toughened with waste particles. *Science and Engineering of Composite Materials, 25*(4), 679-687.

Alsaadi, M., & Erkliğ, A. (2017). A comparative study on mode I and mode II interlaminar behavior of borax and SiC particles toughened S-glass fabric/epoxy composite. *Arabian Journal for Science and Engineering, 42*(11), 4759-4769.

Anderson, T. L. (2005), *Fracture mechanics: fundamentals and applications*, New York: CRC press.

ASTM, E. (1991). *Standard test method for plane-strain fracture toughness of metallic materials*. Annual book of ASTM standards, pp. 506-536.

ASTM, I. (2007). Standard test methods for flexural properties of unreinforced and reinforced plastics and electrical insulating materials. *ASTM D790-07*.

ASTM, I. (2007). Standard test methods for plane-strain fracture toughness and strain energy release rate of plastic materials. *ASTM D5045-99*.

Byun, J. H., Gillespie Jr, J. W., & Chou, T. W. (1990). Mode I delamination of a three-dimensional fabric composite. *Journal of Composite Materials, 24*(5), 497-518.

Callus, P. J., Mouritz, A. P., Bannister, M. K., & Leong, K. H. (1999). Tensile properties and failure mechanisms of 3D woven GRP composites. *Composites Part A: applied science and manufacturing, 30*(11), 1277-1287.

Carolan, D., Kinloch, A. J., Ivankovic, A., Sprenger, S., & Taylor, A. C. (2016). Mechanical and fracture performance of carbon fibre reinforced composites with nanoparticle modified matrices. *Procedia Structural Integrity, 2*, 96-103.

Cholake, S. T., Moran, G., Joe, B., Bai, Y., Raman, R. S., Zhao, X. L., & Bandyopadhyay, S. (2016). Improved Mode I fracture resistance of CFRP composites by reinforcing epoxy matrix with recycled short milled carbon fibre. *Construction and Building Materials, 111*, 399-407.

Danielsson, M. (1996). Toughened rigid foam core material for use in sandwich constructions. *Cellular polymers, 15*(6), 417-435.

De Souza, J. M., Yoshimura, H. N., Peres, F. M., & Schön, C. G. (2012). Effect of sample pre-cracking method and notch geometry in plane strain fracture toughness tests as applied to a PMMA resin. *Polymer Testing, 31*(6), 834-840.

Dransfield, K., Baillie, C., & Mai, Y. W. (1994). Improving the delamination resistance of CFRP by stitching—a review. *Composites Science and Technology, 50*(3), 305-317.

Fishpool, D. T., Rezai, A., Baker, D., Ogin, S. L., & Smith, P. A. (2013). Interlaminar toughness characterisation of 3D woven carbon fibre composites. *Plastics, rubber and composites, 42*(3), 108-114.

Göktaş, D., Kennon, W. R., & Potluri, P. (2017). Improvement of Mode I interlaminar fracture toughness of stitched glass/epoxy composites. *Applied Composite Materials, 24*(2), 351-375.

Gouda, P. S., Kudari, S. K., Prabhuswamy, S., & Jawali, D. (2011). Fracture toughness of glass-carbon (0/90) s fiber-reinforced polymer composite–an experimental and numerical study. *Journal of Minerals and Materials Characterization and Engineering, 10*(8), 671.

Greenhalgh, E. (2009). *Failure analysis and fractography of polymer composites*. Cambridge: 1st ed, Woodhead Publishing.

Guénon, V. A., Chou, T. W., & Gillespie, J. W. (1989). Toughness properties of a three-dimensional carbon-epoxy composite. *Journal of materials science, 24*(11), 4168-4175.

Ji, A. H., Lu, M., Zha, M., Dong, B. Z., Gao, L. H., & Dai, Z. D. (2014). Model I Interlaminar Fracture Toughness of Carbon Fiber-reinforced Polymer Matrix Composites. *Advanced Materials Research, 887*, 81-85.

Karevan, M. (2022). Elastic response of Carbon Black reinforced polyester based composites using micromechanical models: Role of interphase. *Proceedings of the Institution of Mechanical Engineers, Part N: Journal of Nanomaterials, Nanoengineering and Nanosystems*, *236* (3-4), 87-100.

Lo, J., Zhang, R., Shalchi-Amirkhiz, B., Walsh, D., Bolduc, M., Lin, S., & Bielawski, M. (2015). Improving Fracture Toughness of Alumina with Multi-Walled Carbon Nanotube and Alumina Fiber Reinforcements. *Ceramic engineering and science proceedings. Advances in Ceramic Armor XI, 36*(4), 137.

Mouritz, A. P., Baini, C., & Herszberg, I. (1999). Mode I interlaminar fracture toughness properties of advanced textile fibreglass composites. *Composites Part A: Applied Science and Manufacturing, 30*(7), 859-870.

Mouritz, A. P., & Cox, B. N. (2000). A mechanistic approach to the properties of stitched laminates. *Composites part A: applied science and manufacturing, 31*(1), 1-27.

Nakayama, J., Abe, H., & Bradt, R. C. (1981). Crack stability in the work-of-fracture test: refractory applications. *Journal of the American Ceramic Society, 64*(11), 671-675.

Nizami, A. S., Ouda, O. K. M., Rehan, M., El-Maghraby, A. M. O., Gardy, J., Hassanpour, A. & Ismail, I. M. I. (2016). The potential of Saudi Arabian natural zeolites in energy recovery technologies. *Energy, 108*, 162-171.

Pabst, R. F. (1974). *Determination of K Ic-Factors with Diamond-Saw-Cuts in Ceramic Materials. In Fracture mechanics of ceramics*, Boston: Springer, pp. 555-565.

Peret, C. M., & Rodrigues, J. A. (2008). Stability of crack propagation during bending tests on brittle materials. *Ceramica, 54*, 382-387.

Rao, M. P., Sankar, B. V., & Subhash, G. (2009). Effect of Z-yarns on the stiffness and strength of three-dimensional woven composites. *Composites Part B: Engineering, 40*(6), 540-551.

Sharma, S. K., & Sankar, B. V. (1997). Effect of stitching on impact and interlaminar properties of graphite/epoxy laminates. *Journal of Thermoplastic Composite Materials, 10*(3), 241-253.

Shivakumar Gouda, P. S., G Kodancha, K., & Jawali, D. (2013). Experimental and numerical investigations on fracture behavior of high silica glass/satin textile fiber-reinforced hybrid polymer composites. *Advanced Materials Letters, 4*(11), 827-835.

Solaimurugan, S., & Velmurugan, R. (2008). Influence of in-plane fibre orientation on mode I interlaminar fracture toughness of stitched glass/polyester composites. *Composites Science and Technology, 68*(7-8), 1742-1752.

Sreekala, M. S., George, J., Kumaran, M. G., & Thomas, S. (2002). The mechanical performance of hybrid phenol-formaldehyde-based composites reinforced with glass and oil palm fibres. *Composites science and technology, 62*(3), 339-353.

Srivastava, V. K., Gries, T., Veit, D., Quadflieg, T., Mohr, B., & Kolloch, M. (2017). Effect of nanomaterial on mode I and mode II interlaminar fracture toughness of woven carbon fabric reinforced polymer composites. *Engineering Fracture Mechanics, 180*, 73-86.

Stewart, J. K., Mahfuz, H., & Carlsson, L. A. (2010). Enhancing mechanical and fracture properties of sandwich composites using nanoparticle reinforcement. *Journal of materials science, 45*(13), 3490-3496.

Sudheer, M., Pradyoth, K. R., & Somayaji, S. (2015). Analytical and numerical validation of epoxy/glass structural composites for elastic models. *American Journal of Materials Science, 5*(3C), 162-168.

Tan, K. T., Watanabe, N., Sano, M., Iwahori, Y., & Hoshi, H. (2010). Interlaminar fracture toughness of vectran-stitched composites-experimental and computational analysis. *Journal of composite materials, 44*(26), 3203-3229.

Tan, P., Tong, L., & Steven, G. P. (2000). Behavior of 3D orthogonal woven CFRP composites. Part II. FEA and analytical modeling approaches. *Composites Part A: Applied science and manufacturing, 31*(3), 273-281.

Tan, P., Tong, L., Steven, G. P., & Ishikawa, T. (2000). Behavior of 3D orthogonal woven CFRP composites. Part I. Experimental investigation. *Composites Part A: Applied Science and Manufacturing, 31*(3), 259-271.

Tarfaoui, M., & Hamitouche, L. (2012). Mode I interlaminar fracture toughness of through-thickness reinforced laminated structures. *Advanced Materials Research, 423*, 154-165.

Tong, L., Mouritz, A. P., & Bannister, M. K. (2002). *3D fibre reinforced polymer composites*. Elsevier.

Williams, J. G., Pavan, A., & Blackman, B. (Eds.). (2003). *Fracture of Polymers, Composites and Adhesives II: 3rd ESIS TC4 Conference*. Elsevier.

Yee, A. F., & Pearson, R. A. (1986). Toughening mechanisms in elastomer-modified epoxies. *Journal of materials science, 21*(7), 2462-2474.

Zimmermann, E. A., Launey, M. E., & Ritchie, R. O. (2010). The significance of crack-resistance curves to the mixed-mode fracture toughness of human cortical bone. *Biomaterials, 31*(20), 5297-5305